Geophysical Research Letters

RESEARCH LETTER
10.1029/2020GL089982

Modern Meteoric ^{36}Cl Deposition in the Atacama Desert, Chile

Fan Wang[1,2,3] **and Greg Michalski**[2,4]

[1]School of Atmospheric Sciences, Guangdong Province Key Laboratory for Climate Change and Natural Disaster Studies, Sun Yat-sen University, Zhuhai, Guangdong Province, China, [2]Department of Earth, Atmospheric and Planetary Sciences, Purdue University, West Lafayette, IN, USA, [3]Southern Marine Science and Engineering Guangdong Laboratory (Zhuhai), Zhuhai, Guangdong Province, China, [4]Department of Chemistry, Purdue University, West Lafayette, IN, USA

Key Points:

- ^{36}Cl deposition has been measured across a west-east transect in the Atacama Desert, Chile
- Elevated ^{36}Cl dry deposition in the region was attributed to enhanced stratosphere-troposphere transport over the Andes
- Variations in the ^{36}Cl deposition flux along the transect were attributed to chloride displacements by atmospheric acids

Correspondence to:
G. Michalski,
gmichals@purdue.edu

Citation:
Wang, F., & Michalski, G. (2020). Modern meteoric ^{36}Cl deposition in the Atacama Desert, Chile. *Geophysical Research Letters*, *47*, e2020GL089982. https://doi.org/10.1029/2020GL089982

Abstract Modern atmospheric deposition along a west-east transect in the Atacama Desert, Chile, was collected to constrain the meteoric ^{36}Cl/Cl ratio and ^{36}Cl deposition flux. The ^{36}Cl deposition flux had a threefold change, from 3.62(±0.18) to 11.6(±0.2) atoms m^{-2} s^{-1}, going from the coast to the high Andes. The ^{36}Cl deposition was mainly as dry deposition, and the magnitude and differences between sites were attributed to stratosphere-troposphere transport and chloride deficits by acid displacement, respectively. The meteoric ^{36}Cl/Cl ratios varied greatly from 31.5(±1.1) × 10^{-15} to 247(±10) × 10^{-15}, which was attributed to local inputs of oceanic chloride near the coast or chloride minerals entrained from nearby salt playas. This study presented refined estimates of the ^{36}Cl deposition flux and meteoric ^{36}Cl/Cl ratio in a desert region in southern tropical zone. The data set will provide a baseline for using natural ^{36}Cl abundances to date salt accumulation in the Atacama.

Plain Language Summary ^{36}Cl is a radioactive chlorine isotope found in the atmosphere and can be used in many ways, from determining ages of soils and groundwaters to tracing origins of salts and groundwater flow paths. In order to use meteoric ^{36}Cl, we must know how much is deposited from the atmosphere to the surface. There are only a few studies of ^{36}Cl deposition in southern hemisphere, even less in extraordinarily dry environments, which hinders its use in desert regions south of the equator. We have measured the ^{36}Cl deposition along a west-east transect in the Atacama Desert in northern Chile and developed a simple explanation for our results. Future work will use this deposition rate to determine the duration of soil salt accumulation in the Atacama and understand changes in climate (precipitation) in the past.

1. Introduction

Meteoric ^{36}Cl/Cl ratios and ^{36}Cl deposition fluxes to the surface are important biogeochemical tracers because they can be used as chloride source identifiers, to trace hydrologic flow, or as geochronometers. Approximately two thirds of meteoric ^{36}Cl is produced in the stratosphere through the spallation of ^{40}Ar by primary and secondary cosmic rays (Davis & Schaeffer, 1955; Lal & Peters, 1967; Phillips, 2000), which is then transported to the troposphere during episodes of stratosphere-troposphere transport (STT) (Bentley & Davis, 1982; Lal & Peters, 1967; Masarik & Beer, 1999). In the troposphere, meteoric ^{36}Cl mixes with stable chlorine, and they are scavenged to the surface primarily by wet deposition or more slowly via dry deposition. Therefore, meteoric ^{36}Cl/Cl ratios and ^{36}Cl deposition fluxes can be determined by ^{36}Cl production, STT, and local scavenging schemes (Lal & Peters, 1967; Phillips, 2000). Due to its long half-life (301 Kyr) and conservative behavior, meteoric ^{36}Cl has been successfully used to assess atmospheric mixing (Blinov et al., 2000; Johnston & McDermott, 2008), discern chloride sources (Rao et al., 2005; Sherif et al., 2019), and determine ages of groundwater, soils, evaporites, and ice cores (Cartwright et al., 2017; Jannik et al., 1991; Liu et al., 1994; Phillips, 2000; Thompson et al., 1997). Knowledge of worldwide meteoric ^{36}Cl/Cl ratios and ^{36}Cl deposition fluxes is essential in order to utilize meteoric ^{36}Cl in biogeochemical studies, yet the "initial value problem" remains a challenge (Davis et al., 1998).

Advances in ^{36}Cl measurements have enabled the assessment of ^{36}Cl deposition in many regions. Measurements of low-level ^{36}Cl concentrations by the accelerator mass spectrometry (AMS) were first adopted for ^{36}Cl analysis of meteorites, ice cores, or precipitations/water samples to determine ages of

Received 23 JUL 2020
Accepted 20 SEP 2020
Accepted article online 13 OCT 2020

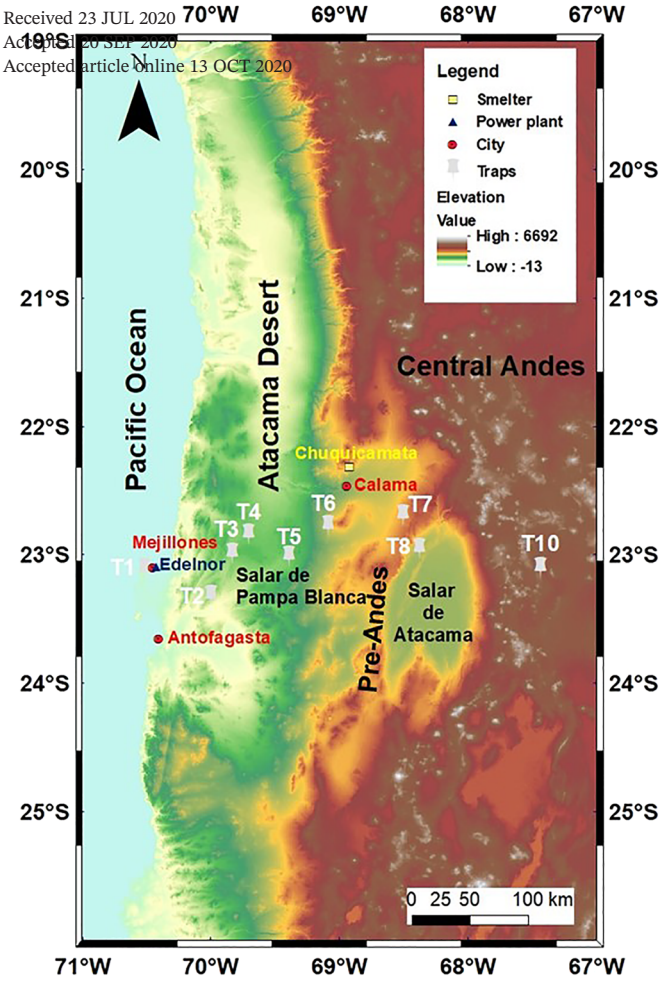

Figure 1. Topographic map of the Atacama Desert and locations of dust traps (adapted from Wang et al., 2014).

meteorites/ice or detect "^{36}Cl bomb pulses" generated by thermonuclear tests in the 1950s (Elmore et al., 1982; Finkel et al., 1980; Nishiizumi et al., 1993; Phillips et al., 1990; Suter et al., 1987; Synal et al., 1990). Later, ^{36}Cl was measured in precipitation of Israel (Herut et al., 1992), the United States (Hainsworth et al., 1994; Knies et al., 1994), Australia (Keywood et al., 1998), Japan (Tosaki et al., 2012), across the Europe (Johnston & McDermott, 2008; Pupier et al., 2016; Santos et al., 2004), and at other places around the planet (Scheffel et al., 1999). Moysey et al. (2003) explored the nationwide ^{36}Cl/Cl ratios of meteoric groundwater to show the spatial patterns of meteoric ^{36}Cl/Cl ratio across the United States. However, on the whole, meteoric ^{36}Cl measurements have been limited, and discrepancies remain between measurements and model estimates. The latter have been obtained by coupling the theoretical calculation of atmospheric production and deposition flux as a function of precipitation (Blinov et al., 2000; Keywood et al., 1998; Phillips, 2000; Pupier et al., 2016; Scheffel et al., 1999). Moreover, the constraints on meteoric ^{36}Cl/Cl ratios or ^{36}Cl deposition fluxes have been mostly studied in middle- to high-latitude regions of northern hemisphere, with only two studies in tropical regions or southern hemisphere by Keywood et al. (1998) and Scheffel et al. (1999). Further, the ^{36}Cl measurements were mainly conducted on precipitation samples, and only a few studies measured the dry deposition of ^{36}Cl, such as in the continental United States where it accounted for ~1/4 of the total ^{36}Cl deposition (Hainsworth et al., 1994; Moysey et al., 2003). However, in desert regions where the role of wet deposition diminishes and dry deposition becomes more important, there have been many studies that have applied meteoric ^{36}Cl (see Phillips, 2000), yet the ^{36}Cl deposition constraints are rare.

This study examines the spatial distributions of ^{36}Cl deposition flux and meteoric ^{36}Cl/Cl ratio across a west-east transect in the Atacama Desert, Chile. The Atacama has widespread salt deposits that are mainly attributed to long-term accumulation of atmospheric deposition under the hyperarid environment (Ewing et al., 2007; Sturchio et al., 2009). Significant chloride accumulation has likely occurred throughout the period of hyperaridity in the Atacama, but there is little consensus on when hyperaridity began. One way to date chloride accumulation is to use meteoric ^{36}Cl with known meteoric ^{36}Cl/Cl ratios or ^{36}Cl deposition fluxes, which would have implications for the aridity history of the Atacama. The Atacama's hyperaridity suggests that salt accumulation by dry deposition is significantly more important than wet deposition, making the Atacama unique relative to most regions where wet deposition dominates. In addition, the Andes has been reported to be a region with uniquely intense STT (Škerlak et al., 2014), some of the highest in the world. Further, despite its remoteness, the Atacama is not free from anthropogenic activities (Wang et al., 2014), but how anthropogenic activities have impacted salt deposition, including chloride, is inadequately investigated. This study furthers our understandings of ^{36}Cl deposition in southern hemisphere tropical zone and in hyperarid environments, where data are limited and there are interesting meteoric ^{36}Cl applications.

2. Methods and Material

The Atacama Desert, Chile, stretches more than 1,000 km along the Pacific coast of South America (20–30°S). The Atacama Desert consists of three major physiographic units from west to east: the Coastal Range, the Central Depression, and the Andes (Ericksen, 1981) (Figure 1). The Coastal Range stretches ~3,000 km along the Pacific coast; the Andes comprises a series of plateaus (~4,000 m in altitude) and a succession of parallel pre-Andean mountain ranges with intervening valleys and basins; the Central Depression is an intermediate depression with minimal precipitation (<2 mm yr^{-1}) extending from ~22°S to 26°S (Houston, 2006).

Salt playa ("salar" in Spanish), formed by drainages from large basins and subsequent evaporation, spread over ~7,250 km^2 in northern Chile as prominent features (Stoertz & Ericksen, 1974).

Atmospheric deposition was collected using an array of nine dust traps set up along a west-east transect across the Atacama (Figure 1) and left exposed from 10 July 2007 to 1 January 2010 (Wang et al., 2014). Each trap (T) was identified as T1 on the Coastal Range, T2–T6 in the Central Depression, and T7–T10 on the Andes (T7: the pre-Andean range, T8: the Atacama Basin, and T10: the Andean Plateau). The sampling transect encompassed the rims of Salar de Pampa Blanca and Salar de Atacama (Figure 1). Each trap consisted of a single-piece Bundt cake pan (outer ring diameter: 25 cm, surface area: 0.05 m^2) fitted with a circular piece of 1/4-inch-mesh galvanized screen on which a layer of pre-washed glass marbles was suspended to mimic desert pavement surfaces (Reheis et al., 1995). The traps were mounted on ~1-m-high poles above the ground to eliminate most saltating particles. Atmospheric deposition samples were recovered by washing the pans, marbles, and mesh with Millipore™ water (resistivity: >18 MΩ·cm) into 1-L plastic bottles. The washing solutions were kept frozen before being shipped to Purdue University overnight and gradually freeze-dried in the lab. In addition, one sample from the Salar de Pampa Blanca was collected to constrain the $^{36}Cl/Cl$ ratios of surface minerals in salt playas. The resulting bulk dust and salar samples were washed with 30-ml Millipore™ water, filtered through a 0.45-μm polytetrafluoroethylene filter to separate the insoluble and soluble fractions. One 3-ml aliquot of the filtrate was analyzed for Na^+ and Cl^- concentrations with <5% uncertainties by Thermo Scientific iCAP 6500 inductively coupled plasma-optical emission spectroscopy (ICP-OES) and Dionex DX-500 ion chromatography (IC), respectively. The ICP-OES and IC data were used to calculate ion deposition rates that were previously reported in Wang et al. (2014).

Based on the measured Cl^- concentrations, another split of each sample was withdrawn from the filtrate and a suitable amount of ^{36}Cl-free chloride carrier was added to obtain enough Cl^- for the $^{36}Cl/Cl$ (Cl: total chlorine, mainly $^{35}Cl + {}^{37}Cl$) measurement (Table 1). $Ba(NO_3)_2$ salt was added to the solution to eliminate SO_4^{2-} as $BaSO_{4(s)}$ since ^{36}S could interfere ^{36}Cl measurements. Excess $AgNO_3$ salt was then added to precipitate $AgCl_{(s)}$, which was then isolated by centrifuging and filtration, washed five times in Millipore™ water, and freeze-dried. The purified $AgCl_{(s)}$ was loaded into a copper target and analyzed by AMS at the Purdue Rare Isotope Measurement (PRIME) laboratory according to the general methodology by Sharma et al. (2000). Dilution of a NIST ^{36}Cl standard (SRM 4422L) with the calibrated $^{36}Cl/Cl$ ratio of 1.537×10^{-10} was used for normalization. Six AMS runs were performed on each sample with precision generally ≤5%. Procedural blanks prepared along with the samples had $^{36}Cl/Cl$ ratios ≤6.9×10^{-15}, and all reported values were blank-corrected (Table 1). The stated error for AMS-measured $^{36}Cl/Cl$ ratio represented 1 standard deviation that was computed as a weighted average of internal (e.g., counting statistics and beam fluctuations) and external (e.g., replicates, standards, and blanks) errors. Meteoric $^{36}Cl/Cl$ ratios were obtained after the correction of AMS-measured $^{36}Cl/Cl$ by subtracting the carrier chloride from the total chloride (Table 1). The ^{36}Cl deposition flux was calculated by multiplying the meteoric $^{36}Cl/Cl$ ratios and chloride deposition rates previously reported in Wang et al. (2014) (Table 1).

3. Results

Meteoric $^{36}Cl/Cl$ ratios varied between sites by approximately eightfold from the lowest of $31.5(\pm1.1) \times 10^{-15}$ at the T1 site to the highest of $247(\pm10) \times 10^{-15}$ at the T4 site (Table 1). The T5, T7, and T8 sites had relatively low meteoric $^{36}Cl/Cl$ ratios of $146(\pm5) \times 10^{-15}$, $180(\pm6) \times 10^{-15}$, and $94.0(\pm2.2) \times 10^{-15}$, respectively, while the meteoric $^{36}Cl/Cl$ ratios at the T2, T3, T6, and T10 sites ranged from $212(\pm4) \times 10^{-15}$ to $234(\pm7) \times 10^{-15}$ (Table 1). The ^{36}Cl deposition flux varied between sites approximately threefold from the lowest of 3.62 ± 0.18 atoms m^{-2} s^{-1} at the T6 site to the highest of 11.6 ± 0.2 atoms m^{-2} s^{-1} at the T10 site. The T8 and T1 sites had the next highest ^{36}Cl deposition fluxes of 7.01 ± 0.16 and 6.64 ± 0.23 atoms m^{-2} s^{-1}, respectively, while the T2–T5 and T7 sites had relatively low ^{36}Cl deposition fluxes ranging from $3.81(\pm0.13)$ to $6.20(\pm0.21)$ atoms m^{-2} s^{-1} (Table 1). The $^{36}Cl/Cl$ ratio of the Salar de Pampa Blanca sample was $18.0(\pm1.8) \times 10^{-15}$.

4. Discussion

We hypothesize that the eightfold change in meteoric $^{36}Cl/Cl$ ratio and the threefold change in ^{36}Cl deposition flux over a relatively narrow geographic transect cannot be attributed to variations in meteoric ^{36}Cl

Geophysical Research Letters

10.1029/2020GL089982

Table 1
Details of AMS Measurement of ^{36}Cl, Deposition Data, As Well As the Calculated Meteoric $^{36}Cl/Cl$ Ratios and ^{36}Cl Deposition Fluxes

	^{36}Cl measurement details					Deposition data[c]						
Site	Sample solution (g)	Cl^- content in sample solutions (mg g^{-1})	^{36}Cl-free carrier[a] (g)	AMS-measured $^{36}Cl/Cl$ ($\times10^{-15}$)	Meteoric $^{36}Cl/Cl$[b] ($\times10^{-15}$)	Cl^- deposition rate (mmol m^{-2} yr^{-1})	Na^+ deposition rate (mmol m^{-2} yr^{-1})	NO_3^- deposition rate (mmol m^{-2} yr^{-1})	Chloride deficit (%)	$Na^+/(Cl^- + NO_3^-)$	Measured ^{36}Cl deposition flux[d] (atoms m^{-2} s^{-1})	$F_{36theor}$ based on Equation 2 (atoms m^{-2} s^{-1})
T1	13.2518	1.206	0	31.5 ± 1.1	31.5 ± 1.1	11.05	23.90	3.47	60.5	1.65	6.64 ± 0.23	6.72
T2	20.3598	0.144	10.0809	48.2 ± 1.9	234 ± 8	1.39	4.13	2.88	66.3	0.97	6.20 ± 0.21	6.36
T3	20.2604	0.106	11.0899	34.4 ± 1.2	234 ± 7	0.96	5.24	4.62	81.7	0.94	4.29 ± 0.14	5.40
T4	20.2236	0.150	9.5782	54.2 ± 2.8	247 ± 10	1.29	4.86	3.54	73.5	1.01	6.08 ± 0.26	5.91
T5	20.1710	0.190	8.6011	41.5 ± 1.8	146 ± 5	1.73	6.77	4.83	74.4	1.03	4.82 ± 0.16	5.85
T6	20.1982	0.088	11.1269	27.9 ± 1.5	223 ± 11	0.85	5.75	3.70	85.2	1.26	3.62 ± 0.18	5.18
T7	20.2813	0.122	10.1365	32.2 ± 1.2	180 ± 6	1.11	3.48	2.74	68.1	0.90	3.81 ± 0.13	6.25
T8	20.2262	0.413	4.9603	56.4 ± 1.8	94.0 ± 2.2	3.91	5.49	2.00	28.8	0.93	7.01 ± 0.16	8.70
T10	20.2458	0.287	6.6972	92.3 ± 2.3	212 ± 4	2.86	2.20	0.54	−30.0	0.65	11.6 ± 0.2	N.A.
Salar	N.A.	N.A.	0	18.0 ± 1.8	18.0 ± 1.8	N.A.	N.A.	N.A.	N.A.	N.A.	N.A.	N.A.

Note. N.A. = not applicable.
[a]The Cl^- concentration in the ^{36}Cl-free chloride carrier is 1.121 ± 0.001 mg g^{-1}. [b]Propagated uncertainties from uncertainties in Cl^- content in sample solution (±0.001 mg g^{-1}) and carrier as well as AMS analytical errors. [c]The deposition data were previously reported in Wang et al. (2014). [d]Propagated uncertainties from uncertainties in meteoric $^{36}Cl/Cl$ ratios and Cl^- deposition rates (±0.01 mmol m^{-2} yr^{-1}).

production, but variations in chloride sources and local atmospheric processing, respectively. This is because the solar activity and interplanetary (or Earth's) magnetic field that together determine ^{36}Cl production in the atmosphere can be considered invariant along our ~320-km-wide sampling transect. The ocean and salt playas are two major terrestrial chloride sources (Li et al., 2019; Moysey et al., 2003; Wang et al., 2014), and the terrestrial chlorides typically have very low ^{36}Cl activities because of the 1–2 orders of magnitude slower in situ ^{36}Cl production compared to meteoric ^{36}Cl production and the non-stop radioactive decay of ^{36}Cl (Fifield et al., 2013; Phillips, 2000). Therefore, inputs of terrestrial chloride of very low ^{36}Cl activities can potentially lower meteoric ^{36}Cl/Cl ratios (Moysey et al., 2003). The ^{36}Cl deposition flux, on the other hand, should be relatively insensitive to local terrestrial sources but mainly impacted by atmospheric processes such as STT, and chloride displacement by atmospheric acids (Wang et al., 2014).

4.1. Distribution of ^{36}Cl Deposition Flux

The largest ^{36}Cl deposition flux (11.6 ± 0.2 atoms m^{-2} s^{-1}) at the T10 site is about two times more than the ^{36}Cl deposition flux estimated by the model by Phillips (2000). The estimated ^{36}Cl deposition flux ($F_{36}(P, \lambda)$) mainly depends on ^{36}Cl production, and precipitation rate:

$$F_{36}(P,\lambda) = F_{36}(\lambda)\left[1 + \frac{S_F(\lambda_0)}{F_{36}(\lambda_0)}\left(P - \overline{P}(\lambda)\right)\right] \quad (1)$$

where $F_{36}(\lambda)$ is the average ^{36}Cl deposition flux as a function of latitude (λ), $S_F(\lambda_0)$ is the slope of the ^{36}Cl deposition flux versus precipitation rate determined at the latitude λ_0, $F_{36}(\lambda_0)$ is the average ^{36}Cl deposition flux at the latitude λ_0, P is the precipitation rate at the study site, and $\overline{P}(\lambda)$ is the average precipitation rate for the latitude (λ) belt. Since T10 is at 23.10°S, $F_{36}(\lambda)$ was taken as 22.5 atoms m^{-2} s^{-1} from Phillips (2000) and $\overline{P}(\lambda)$ was taken as 795 mm yr^{-1} from Baumgartner and Reichel (1975). P near the T10 site during 2007–2009 was reported to be 50 mm yr^{-1} as snow (DGA, 2010). $S_F(\lambda_0)/F_{36}(\lambda_0)$ was taken as 1.11 × 10^{-3} yr mm^{-1} based on Phillips (2000) using data mainly from Knies et al. (1994), Hainsworth et al. (1994), and Keywood et al. (1998). This yielded an estimated ^{36}Cl deposition flux of 3.89 atoms m^{-2} s^{-1} at the T10 site, three times less than the measurement (11.6 ± 0.2 atoms m^{-2} s^{-1}).

We suggest that the discrepancy between the modeled and measured ^{36}Cl deposition flux at the T10 site may be because of the neglection of strong STT around the Andes. The Andean range induces significant STT (Škerlak et al., 2014) due to upper tropospheric turbulence caused by breaking mountain waves (Lamarque et al., 1996; Worthington, 1998). Using the ERA-Interim reanalysis data set, Škerlak et al. (2014) compiled a global climatology of STT from 1979 to 2011 to find seasonal STT hotspots over the Andes. During September to February, the STT air mass flux was on the order of 500 kg km^{-2} s^{-1} over the Andes, the highest in southern hemisphere and among the highest on Earth. Further, due to tall boundary layer heights over tropical deserts (von Engeln & Teixeira, 2013), the Andes region had the most "deep STT events" in southern hemisphere, during which stratospheric air reaches the boundary layer (Škerlak et al., 2014). Stratospheric ^{36}Cl should be predominantly in the form of $HCl_{(g)}$ (Wahlen et al., 1991) due to the highly acidic nature of stratospheric aerosols (cf. Kremser et al., 2016). Stratospheric ^{36}Cl carried into the troposphere during STT events could react on existing aerosols such as mineral dust (Tobo et al., 2009), coat aerosol surfaces (externally mixed), absorb into deliquesced aerosols (Wang et al., 2015), or exchange with existing chloride aerosols (Lal & Peters, 1967), before depositing to the surface. Therefore, a higher ^{36}Cl deposition flux at the T10 site than the model estimate based on Equation 1 may be due to the significant regional STT that is not accounted for by the models of Phillips and others (Lal & Peters, 1967; Parrat et al., 1996; Phillips, 2000).

The ^{36}Cl deposition fluxes at the T1–T8 sites, ranging from 3.62(±0.18) to 7.01(±0.16) atoms m^{-2} s^{-1}, were 39–69% lower than at the T10 site (Table 1), which could be partially due to the lack of precipitation. During 2007–2009, fog deposition of ~22 L m^{-2} yr^{-1} (~22 mm yr^{-1} of precipitation equivalent) at the T1 site (Wang et al., 2014) and rainfall of ~10 mm yr^{-1} at T7 and T8 sites occurred, while no precipitation was recorded at the T2–T6 sites (DGA, 2010). Using Equation 1, the ^{36}Cl deposition flux was estimated to be 2.64–3.19 atoms m^{-2} s^{-1} at the T1–T8 sites, about half of the measured 3.62(±0.18)–7.01(±0.16) atoms m^{-2} s^{-1} (Table 1), supporting the hypothesis of elevated regional STT. However, the model estimates for the T1–T8 sites are only slightly less than that for the T10 site, suggesting that precipitation alone cannot account for the significantly lower ^{36}Cl deposition flux measurements at the T1–T8 sites relative to T10 site. Instead, a correlation

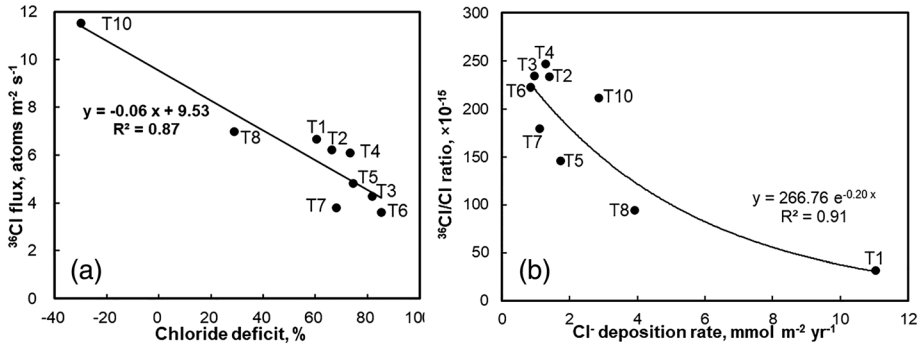

Figure 2. Relationships between the measured ^{36}Cl deposition fluxes and chloride deficits (a), as well as between meteoric ^{36}Cl/Cl ratios and Cl^- deposition rates (b).

between ^{36}Cl deposition fluxes and chloride deficits (Figure 2a) might offer a mechanistic explanation for the differences between model estimates and measurements.

When aerosol chloride reacts with atmospheric acids such as $HNO_{3(g)}$ and $H_2SO_{4(g)}$, the more volatile acid $HCl_{(g)}$ is liberated resulting in the loss of chloride (both ^{36}Cl and stable chlorine) from aerosols (Newberg et al., 2005). This was often referred to as a "chloride deficit" and commonly observed in aerosols along the coastal regions near large cities (Harkel, 1997; Newberg et al., 2005). Our previous work indicated that sea-salt aerosols (SSAs) and surface halite (NaCl) minerals were the dominant sources of chloride at the T1 and T2–T8 sites, respectively (Wang et al., 2014). The initial Cl^-/Na^+ molar ratio, prior to acid replacement reactions, is 1.17 at the T1 site as SSAs (the same as seawater) or 1.0 at the T2–T8 sites as halite mineral. The chloride deficits ($\%Cl_{deficit}$) were then calculated as $\{1 - Cl^-/[Na^+ \times (Cl^-/Na^+)_{initial}]\} \times 100\%$, achieving 28.8% to 85.2% for the T1–T10 sites (Table 1) as reported in Wang et al. (2014). Because of $Na^+/(Cl^- + NO_3^-)$ of 1.0 ± 0.1 at the T2–T8 sites (Wang et al., 2014), $HNO_{3(g)} + NaCl_{(s)} \rightarrow NaNO_{3(s)} + HCl_{(g)}$ could be the dominant chloride deficit mechanism. This $HNO_{3(g)}$ was photochemically produced from anthropogenic NO_x generated by transport and power/chemical plants, which was confirmed by a high ^{17}O excess with $\Delta^{17}O$ of ~28‰ (Ewing et al., 2007; Michalski et al., 2003; Wang et al., 2014).

The effect of the chloride deficit was then accounted for in the model estimation of ^{36}Cl deposition flux. First, the average difference in the modeled ^{36}Cl deposition flux between the T1–T8 sites and the T10 site is 1.12 atoms m^{-2} s^{-1}, which is subtracted from the measurement of 11.6 ± 0.2 atoms m^{-2} s^{-1} at T10 to determine the gross ^{36}Cl deposition flux at T1–T8 sites ($F_{36gross}$), achieving 10.5 atoms m^{-2} s^{-1}. The $F_{36gross}$ is the ^{36}Cl dry deposition flux expected without chloride deficits, significantly higher than the measurements of 3.62–7.01 atoms m^{-2} s^{-1} at T1–T8 sites. There is a negative correlation between the measured ^{36}Cl deposition fluxes (F_{36meas}, atoms m^{-2} s^{-1}) and $\%Cl_{deficit}$: $F_{36meas} = -0.06 \times \%Cl_{deficit} + 9.53$ ($n = 9$, $R^2 = 0.87$, $p < 0.01$) (Figure 2a). Instead, no partial correlation ($p > 0.05$) existed between F_{36meas} and precipitation rates with chloride deficit effect removed, suggesting in regions where dry deposition is dominant, precipitation does not directly influence ^{36}Cl deposition fluxes. Thus, Equation 1 was adapted to account for the dependence on chloride deficits for the T1–T8 sites (≤10 mm yr^{-1}):

$$F_{36theor} = F_{36gross} + S_F(\%Cl_{deficit}) \times \%Cl_{deficit} \quad (2)$$

where $S_F(\%Cl_{deficit})$ is the slope (−0.06) of the F_{36meas} versus $\%Cl_{deficit}$. The $F_{36theor}$ at T1–T8 sites were then obtained in the range of 5.18–8.70 atoms m^{-2} s^{-1}, generally in agreement with the measurements (Table 1). Next, we would briefly discuss possible local variables that might cause small deviations between F_{36meas} and $F_{36theor}$ at each site.

4.1.1. The Coastal Site T1

The F_{36meas} of 6.64 ± 0.23 atoms m^{-2} s^{-1} at the T1 site is consistent with $F_{36theor}$ of 6.62 atoms m^{-2} s^{-1}, though this site is heavily influenced by significant SSA deposition and fog deposition. Assuming that the chloride deposition at the T1 site was primarily from SSAs, the ^{36}Cl deposition flux contributed by the ocean was calculated to be 0.15 atoms m^{-2} s^{-1} by multiplying the global average ^{36}Cl/Cl ratio for oceanic chloride

of 0.71(±0.08) × 10^{-15} (Fifield et al., 2013) and the chloride deposition rate of 11.05 mmol m^{-2} yr^{-1} (Wang et al., 2014). This is only ~2% of the measurement, suggesting trivial contribution of SSAs to ^{36}Cl deposition flux at the T1 site. Coastal fog of ~22 L m^{-2} yr^{-1} could have contributed to ^{36}Cl deposition since fog can scavenge both aerosols (with chloride deficits) and atmospheric gases (including the displaced $HCl_{(g)}$), leading to no chloride deficits in local fog (Wang et al., 2014) as found in other studies (e.g., Kikuchi et al., 2009). However, there was a significant chloride deficit (60.5%, Table 1) in deposition at the T1 site, indicating the dominance of dry deposition of aerosols at T1. The large chloride deficit and relatively small ^{36}Cl deposition flux at the T1 site may be due to sizeable emissions of NO_x and SO_2 from power/chemical plants and transport, associated with nearby cities of Mejillones and Antofagasta (Wang et al., 2014).

4.1.2. The Inland Sites T2–T6

The F_{36meas} at the T2–T6 sites (3.62(±0.18)–6.20(±0.21) atoms m^{-2} s^{-1}) (Table 1) were lower than $F_{36theor}$ except at the T1, T2, and T4 sites (Table 1), likely due to the divergence in size fractions for ^{36}Cl and stable chlorine. While stable chlorine may preferably accumulate on coarse aerosols that originate from sea sprays or surface mineral dust (Li et al., 2019; Wang et al., 2014), ^{36}Cl mainly produced in the stratosphere tends to become associated with fine aerosols that are susceptible to downward transport during STT. This could explain while the chloride deposition rate decreased by an order of magnitude from the coastal T1 site to the inland T2–T6 sites (Table 1), the F_{36meas} at T2 (6.20 ± 0.21 atoms m^{-2} s^{-1}) was only slightly lower than at the T1 site (6.64 ± 0.23 atoms m^{-2} s^{-1}). However, fine aerosols were reported to have substantially larger chloride deficits (~90%) than coarse aerosols (~30%) due to larger surface to volume ratios (Harkel, 1997; Hsu et al., 2007), suggesting a confounding role of aerosol size distribution in affecting atmospheric ^{36}Cl inventory. Therefore, the overestimations of F_{36meas} based on Equation 2 (Table 1) at the T3, T5, and T6 sites might reflect more contributions of fine aerosols with larger chloride deficits, with uncertainties derived from corrections using bulk chloride deficits. Nevertheless, the lowest F_{36meas} at the T6 (3.62 ± 0.18 atoms m^{-2} s^{-1}) and T3 (4.29 ± 0.14 atoms m^{-2} s^{-1}) sites were associated with their largest chloride deficits (T6: 85.2%, T3: 81.7%), which were mainly accounted for by NO_x emissions from Calama city and Chuquicamata smelter (~50 km to the north) near the T6 site and roads ~2 km away from the T3 site (Li et al., 2019; Wang et al., 2014).

4.1.3. The Pre-Andean Sites T7–T8

The pre-Andean T7 or T8 sites had precipitation rates of ~10 mm yr^{-1} during 2007–2009 (DGA, 2010; Houston, 2006). The T7 site had the second lowest F_{36meas} of 3.81 ± 0.13 atoms m^{-2} s^{-1}, which was associated with the still significant chloride deficit (68.1%, Table 1) and its lowest bulk dust and salt deposition rates among all the trap sites (Wang et al., 2014). The higher F_{36meas} of 7.01 ± 0.16 atoms m^{-2} s^{-1} at the T8 site was likely a result of lower chloride deficit (28.8%). However, the significantly lower F_{36meas} at the T7 and T8 sites than $F_{36theor}$ of 6.25 and 8.70 atoms m^{-2} s^{-1}, respectively, could also be due to divergences in the chloride deficit between ^{36}Cl-laden fine aerosols and stable chlorine-rich coarse aerosols as stated above.

4.1.4. The Andean Site T10

The largest F_{36meas} (11.6 ± 0.2 atoms m^{-2} s^{-1}) occurred at the T10 site, likely a consequence of strong STT and enhanced precipitation on the Andes as noted earlier. T10 did not have a chloride deficit, but a chloride surplus (i.e., chloride deficit: −30.0%), evidencing that not all chloride in deposition at the T10 site was associated with Na^+, but some with Ca^{2+} (Wang et al., 2014). The NO_3^- deposition rate at the T10 site was ~4–9 times lower compared to at the other sites (Table 1), suggesting that NO_x or $HNO_{3(g)}$ did not effectively transport from the lowlands to this altitude (4,260 m), and therefore, F_{36meas} at T10 was least impacted by the chloride deficit.

4.2. Distribution of Meteoric ^{36}Cl/Cl Ratio in the Atacama

While variations in the ^{36}Cl deposition flux were attributed to regional STT, precipitation, and chloride deficits, variations in the meteoric ^{36}Cl/Cl ratio were mainly attributed to differences in local chloride sources. This is evidenced by the significant exponential correlation between meteoric ^{36}Cl/Cl ratios and chloride deposition rates at the T1–T10 sites (n=9, $R^2 = 0.91$, $p < 0.01$) (Figure 2b). The meteoric ^{36}Cl/Cl ratio at the T1 site (~6 km from the Pacific Ocean) of 31.5 ± 1.1 × 10^{-15} was lowest, corresponding to the highest chloride deposition rate of 11.05 mmol m^{-2} yr^{-1}, which was attributed to the dilution by dry deposition of SSAs with a global average ^{36}Cl/Cl ratio of 0.71(±0.08) × 10^{-15} (Fifield et al., 2013). The inland T2–T6 sites, except T5, had similar meteoric ^{36}Cl/Cl ratios ranging from 223(±11) × 10^{-15} to 247(±10) × 10^{-15} (Table 1).

Since there was no recorded precipitation at the T2–T6 sites during 2007–2009 (DGA, 2010), these meteoric $^{36}Cl/Cl$ ratios could be interpreted as the $^{36}Cl/Cl$ ratios of dry deposition. The T5 site had a significantly lower meteoric $^{36}Cl/Cl$ ratio ($146(\pm5) \times 10^{-15}$), which was attributed to its proximity (~7.5 km to the southwest) to Salar de Pampa Blanca (Stoertz & Ericksen, 1974; Wang et al., 2014) (Figure 1). The surface mineral in the crusts of Salar de Pampa Blanca had a low $^{36}Cl/Cl$ ratio of $18.0(\pm1.8) \times 10^{-15}$ (Table 1), close to the reported $^{36}Cl/Cl$ ratios for Atacamite minerals of 11.1×10^{-15}–28.0×10^{-15} (Reich et al., 2008), but lower than the secular equilibrium $^{36}Cl/Cl$ ratios of 53×10^{-15} for vertical vein fill and 87×10^{-15} for shallow groundwater in the same Baquedano region of the Atacama (Sturchio et al., 2009). The salar could act, in a fashion similar to the ocean, as a local source of chloride as mineral dust that is entrained and deposited nearby, lowering local $^{36}Cl/Cl$ ratios. However, dry deposition of 10–100 μm of particles (Seinfeld & Pandis, 2006) is dominated by gravitational settling; thus, reworking of surface chloride minerals from Salar de Pampa Blanca would mainly impact the nearby T5 rather than the other traps. Likewise, the meteoric $^{36}Cl/Cl$ ratios at the T7 ($180 \pm 6 \times 10^{-15}$) and T8 ($94.0 \pm 2.2 \times 10^{-15}$) sites were relatively low, likely a consequence of the proximities to two nearby open-pit mines south of the T7 site and the Salar de Atacama (Li et al., 2019). The Salar de Atacama, the region's largest halite-type salt playa dating back to the Oligocene-Miocene boundary (Stoertz & Ericksen, 1974), is to the southeast of the T7 (~35-km distance) and T8 (on the salar rim) sites. The surface minerals in the open-pit mines or the Salar de Atacama were not measured for $^{36}Cl/Cl$ ratios that, however, could be reasonably low. This is because the saline groundwaters accounting for the formation of surface chloride minerals in mines or salars are old (Corenthal et al., 2016), and once chloride entered the minerals at depths, the production of ^{36}Cl was limited, but decay did not cease (Reich et al., 2008). While the T10 site also had a relatively high chloride deposition rate (2.86 mmol m^{-2} yr^{-1}), likely accounted for by the nearby Tara lake that had the Cl^- content of ~10 mmol L^{-1} and desiccated seasonally (Wang et al., 2014), its higher $^{36}Cl/Cl$ ratios than those at the T5, T7, and T8 sites were due to the large ^{36}Cl deposition flux facilitated by strong STT and enhanced precipitation.

5. Conclusion

This study constrained the meteoric $^{36}Cl/Cl$ ratios and ^{36}Cl deposition flux along a west-east transect across the Atacama Desert, Chile. The measured ^{36}Cl deposition flux ranged from 3.62 ± 0.18 to 11.6 ± 0.2 atoms m^{-2} s^{-1}, mainly from dry deposition, and are some of the lowest in the world, despite the influence of STT over the Andes. Variations in the ^{36}Cl deposition flux along the transect were mainly attributed to chloride deficits by acid displacement. The meteoric $^{36}Cl/Cl$ ratios varied eightfold across the transect, from $31.5 (\pm1.1) \times 10^{-15}$ to $247(\pm10) \times 10^{-15}$, which was attributed to local inputs of chloride from the Pacific Ocean or surrounding salars. This study provides a baseline for the ^{36}Cl dry deposition in southern hemisphere tropical region and in hyperarid regions, where there are promising applications of meteoric ^{36}Cl as a potential tracer of local STT and duration of salt accumulation.

Data Availability Statement

All data are available in this manuscript or Wang et al. (2014).

Acknowledgments

This work was supported by the National Science Foundation Grant (EAR 0922114) to GM, the Fundamental Research Funds for the Central Universities from Sun Yat-sen University (19lgpy30) and Guangdong Province Key Laboratory for Climate Change and Natural Disaster Studies (2020B1212060025) to FW, as well as several fellowships from Purdue University (Purdue Climate Change Research Center fellowship, Purdue Research Foundation research assistantship, and Purdue Bilsland Dissertation fellowship) to FW. We thank Ji-Hye Seo, Brenda Bowen, and Raul Ochoa for assistance in the field, and the Purdue Rare Isotope Measurement Laboratory (PRIME Lab) for measurements.

References

Baumgartner, A., & Reichel, E. (1975). *World water balance: Mean annual global, continental and maritime precipitation, evaporation and run-off*. Amsterdam: Elsevier.

Bentley, H. W., & Davis, S. N. (1982). Applications of AMS to hydrology. In M. Kutschera (Ed.), *2nd annual symposium on accelerator mass spectrometry* (pp. 193–227). USA: Argonne National Laboratories.

Blinov, A., Massonet, S., Sachsenhauser, H., Stan-Sion, C., Lazarev, V., Beer, J., et al. (2000). An excess of ^{36}Cl in modern atmospheric precipitation. *Nuclear Instruments and Methods in Physics Research B*, *172*(1–4), 537–544. https://doi.org/10.1016/S0168-583X(00)00336-0

Cartwright, I., Cendón, D., Currell, M., & Meredith, K. (2017). A review of radioactive isotopes and other residence time tracers in understanding groundwater recharge: Possibilities, challenges, and limitations. *Journal of Hydrology*, *555*, 797–811. https://doi.org/10.1016/j.jhydrol.2017.10.053

Corenthal, L. G., Boutt, D. F., Hynek, S. A., & Munk, L. A. (2016). Regional groundwater flow and accumulation of a massive evaporite deposit at the margin of the Chilean Altiplano. *Geophysical Research Letters*, *43*, 8017–8025. https://doi.org/10.1002/2016GL070076

Davis, R., & Schaeffer, O. A. (1955). Chlorine-36 in nature. *Annals of the New York Academy of Sciences*, *62*, 107–121. https://doi.org/10.1111/j.1749-6632.1955.tb35368.x

Davis, S. N., Cecil, D., Zreda, M., & Sharma, P. (1998). Chlorine-36 and the initial value problem. *Hydrogeological Journal*, *6*, 104–114. https://doi.org/10.1007/s100400050137

Dirección General de Aguas (DGA) (2010). Actualización de la Evaluación de la Disponibilidad de Recursos Hídricos para Constituir Derechos de Aprovechamiento en las Subcuencas Afluentes al Salar de Atacama. II region, Santiago, Chile (in Spanish).

Elmore, D., Tubbs, L. E., Newman, D., Ma, X. Z., Finkel, R., Nishiizumi, K., et al. (1982). ^{36}Cl bomb pulse measured in a shallow ice core from Dye 3, Greenland. *Nature*, *300*, 735–737. https://doi.org/10.1038/300735a0

Ericksen, G. E. (1981). Geology and origin of the Chilean nitrate deposits. U.S. Geological Survey Professional Paper 1188.

Ewing, S., Michalski, G., Thiemens, M., Quinn, R., Macalady, J., Kohl, S., et al. (2007). Rainfall limit of the N cycle on Earth. *Global Biogeochemical Cycles*, *21*, GB3009. https://doi.org/10.1029/2006GB002838

Fifield, L. K., Tims, S. G., Stone, J. O., Argento, D. C., & De Cesare, M. (2013). Ultra-sensitive measurements of ^{36}Cl and ^{236}U at the Australian National University. *Nuclear Instruments and Methods in Physics Research B*, *294*, 126–131. https://doi.org/10.1016/j.nimb.2012.04.028

Finkel, R. C., Nishiizumi, K., Elmore, D., Ferraro, R. D., & Gove, H. E. (1980). ^{36}C1 in polar ice, rainwater and seawater. *Geophysical Research Letters*, *7*, 983–986. https://doi.org/10.1029/GL007i011p00983

Hainsworth, L. J., Mignerey, A. C., Hclz, G. R., Sharma, P., & Kubik, P. W. (1994). Modern chlorine-36 deposition in southern Maryland, USA. *Nuclear Instruments and Methods in Physics Research B*, *92*(1–4), 345–349. https://doi.org/10.1016/0168-583X(94)96032-1

Harkel, M. T. (1997). The effects of particle-size distribution and chloride depletion of sea-salt aerosols on estimating atmospheric deposition at a coastal site. *Atmospheric Environment*, *31*, 417–427. https://doi.org/10.1016/S1352-2310(96)00249-X

Herut, B., Starinsky, A., Katz, A., Paul, M., Boaretto, E., & Berkovits, D. (1992). ^{36}Cl in chloride-rich rainwater, Israel. *Earth and Planetary Science Letters*, *109*(1–2), 179–183. https://doi.org/10.1016/0012

Houston, J. (2006). Variability of precipitation in the Atacama Desert: Its causes and hydrological impact. *International Journal of Climatology*, *26*, 2181–2198. https://doi.org/10.1002/joc.1359

Hsu, S. C., Liu, S. C., Kao, S. J., Jeng, W. L., Huang, Y. T., Tseng, C. M., et al. (2007). Water-soluble species in the marine aerosol from the northern South China Sea: High chloride depletion related to air pollution. *Journal of Geophysical Research*, *112*, D19304. https://doi.org/10.1029/2007JD008844

Jannik, N., Phillips, F., Smith, G., & Elmore, D. (1991). A ^{36}Cl chronology of lacustrine sedimentation in the Pleistocene Owens River system. *Geological Society of America Bulletin*, *103*, 1146–1159. https://doi.org/10.1130/0016-7606(1991)103%3C1146:ACCOLS%3E2.3.CO;2

Johnston, V. E., & McDermott, F. (2008). The distribution of meteoric ^{36}Cl in precipitation across Europe in spring 2007. *Earth and Planetary Science Letters*, *275*(1–2), 154–164. https://doi.org/10.1016/j.epsl.2008.08.021

Keywood, M. D., Fifield, L. K., Chivas, A. R., & Cresswell, R. G. (1998). Fallout of chlorine 36 to the Earth's surface in the southern hemisphere. *Journal of Geophysical Research*, *103*(D7), 8281–8286. https://doi.org/10.1029/97JD03125

Kikuchi, R., Takada, M., Hifumi, K., Yoshimura, K., Ozeki, T., Kimoto, T., et al. (2009). The degree of Cl-loss for the particulate matter (PM) and fog water sampled at the same air mass at the Hachimantai mountain range in northern Japan. *Atmosperic Research*, *94*, 501–509. https://doi.org/10.1016/j.atmosres.2009.08.001

Knies, D. L., Elmore, D., Sharma, P., Vogt, S., Li, R., Lipschutz, M. E., et al. (1994). ^{7}Be, ^{10}Be and ^{36}Cl in precipitation. *Nuclear Instruments and Methods in Physics Research B*, *92*, 340–344. https://doi.org/10.1016/0168-583X(94)96031-3

Kremser, S., Thomason, L. W., von Hobe, M., Hermann, M., Deshler, T., Timmreck, C., et al. (2016). Stratospheric aerosol—Observations, processes, and impact on climate. *Reviews of Geophysics*, *54*, 278–335. https://doi.org/10.1002/2015RG000511

Lal, D., & Peters, B. (1967). Cosmic-ray produced radioactivity on the Earth. *Handbook of Physics*, *46*, 551–612. https://doi.org/10.1007/978-3-642-46079-1_7

Lamarque, J. F., Langforda, A. O., & Proffitt, M. H. (1996). Cross-tropopause mixing of ozone through gravity wave breaking: Observation and modelling. *Journal of Geophysical Research*, *101*(D17), 22,969–22,976. https://doi.org/10.1029/96JD02442

Li, J., Wang, F., Michalski, G., & Wilkins, B. (2019). Atmospheric deposition across the Atacama Desert, Chile: Compositions, source distributions, and interannual comparisons. *Chemical Geology*, *525*, 435–446. https://doi.org/10.1016/j.chemgeo.2019.07.037

Liu, B., Phillips, F. M., Elmore, D., & Sharma, P. (1994). Depth dependence of soil carbonate accumulation based on cosmogenic ^{36}Cl dating. *Geology*, *22*, 1071–1074. https://doi.org/10.1130/0091-7613(1994)022%3C1071:DDOSCA%3E2.3.CO;2

Masarik, J., & Beer, J. (1999). Simulation of particle fluxes and cosmogenic nucleid production in the Earth's atmosphere. *Journal of Geophysical Research*, *104*, 12,099–12,111. https://doi.org/10.1029/1998JD200091

Michalski, G., Scott, Z., Kabiling, M., & Thiemens, M. (2003). First measurements and modeling of ^{17}O in atmospheric nitrate. *Geophysical Research Letters*, *30*(D10), 1870. https://doi.org/10.1029/2003GL017015

Moysey, S., Davis, S. N., Zreda, M., & Cecil, L. D. W. (2003). The distribution of meteoric ^{36}Cl/Cl in the United States: A comparison of models. *Hydrogeological Journal*, *11*, 615–627. https://doi.org/10.1007/s10040-003-0287-z

Newberg, J. T., Matthew, B. M., & Anastasio, C. (2005). Chloride and bromide depletions in sea-salt particles over the northeastern Pacific Ocean. *Journal of Geophysical Research*, *110*, D06209. https://doi.org/10.1029/2004JD005446

Nishiizumi, K., Arnold, J. R., Elmore, D., Ma, X., Newman, D., & Gove, H. E. (1993). ^{36}Cl and ^{53}Mn in Antarctic meteorites and ^{10}Be-^{36}Cl dating of Antarctic ice. *Earth and Planetary Science Letters*, *62*, 407–417.

Parrat, Y., Hajdas, W., Baltensperger, U., Synal, H. A., Kubik, P. W., Gaggeler, H. W., & Suter, M. (1996). Atmospheric production rates of ^{36}Cl. In U. Baltensperger & R. Lorenzen (Eds.), *Paul Scherrer Institut, Annual Report 1996, Annex IIIA*. Switzerland: Villigen.

Phillips, F. M. (2000). Chlorine-36. In P. G. Cook & A. L. Herczeg (Eds.), *Environmental tracers in subsurface hydrology*. Boston: Springer. https://doi.org/10.1007/978-1-4615-4557-6_10

Phillips, F. M., Davis, S. N., & Kubik, P. (1990). A proposal to use chlorine-36 for monitoring the movement of radionuclides from nuclear explosions. *Ground Water Monitoring and Remediation*, *10*(3), 106–113. https://doi.org/10.1111/j.1745-6592.1990.tb00009.x

Pupier, J., Benedetti, L., Bouchez, C., Bourles, D., Leclerc, E., Thiry, Y., Guillou, V., & ASTER Team (2016). Monthly record of the Cl and ^{36}Cl fallout rates in a deciduous forest ecosystem in NE France in 2012 and 2013. *Quaternary Geochronology*, *35*, 26–35. https://doi.org/10.1016/j.quageo.2016.04.002

Rao, U., Hollocher, K., Sherman, J., Eisele, I., Frunzi, M. N., Swatkoski, S. J., & Hammons, A. L. (2005). The use of ^{36}Cl and chloride/bromide ratios in discerning salinity sources and fluid mixing patterns: A case study at Saratoga Springs. *Chemical Geology*, *222*, 94–111. https://doi.org/10.1016/j.chemgeo.2005.06.011

Reheis, M. C., Goodmacher, J. C., Harden, J. W., McFadden, L. D., Rockwell, T. K., Rockwell, T. K., et al. (1995). Quaternary soils and dust deposition in southern Nevada and California. *Geological Society of America Bulletin*, *107*, 1003. https://doi.org/10.1130/0016-7606(1995)107%3C1003:QSADDI%3E2.3.CO;2

Reich, M., Palacios, C., Parada, M. A., Fehn, U., Cameron, E. M., Leybourne, M. I., & Zúñiga, A. (2008). Atacamite formation by deep saline waters in copper deposits from the Atacama Desert, Chile: Evidence from fluid inclusions, groundwater geochemistry, TEM, and ^{36}Cl data. *Mineralium Deposita*, *43*, 663–675. https://doi.org/10.1007/s00126-008-0184-4

Santos, F., Lopez-Gutierrez, J., Garcıa-Leon, M., Schnabel, C., Synal, H. A., & Suter, M. (2004). Analysis of ^{36}Cl/Cl in atmospheric samples from Seville (Spain) by AMS. *Nuclear Instruments and Methods in Physics Research B*, *223–224*, 501–506. https://doi.org/10.1016/j.nimb.2004.04.094

Scheffel, C., Blinov, A., Massonet, S., Sachsenhauser, H., Stan-Sion, C., Beer, J., et al. (1999). ^{36}Cl in modern atmospheric precipitation. *Geophysical Research Letters*, *26*(10), 1401–1404. https://doi.org/10.1029/1999GL900249

Seinfeld, J. H., & Pandis, S. N. (2006). *Atmospheric chemistry and physics: From air pollution to climate change*. New York: John Wiley & Sons.

Sharma, P., Bourgeois, M., Elmore, D., Granger, D., Lipschutz, M. E., Ma, X., et al. (2000). PRIME lab AMS performance, upgrades and research applications. *Nuclear Instruments and Methods in Physics Research B*, *172*, 112–123. https://doi.org/10.1016/S0168-583X(00)00132-4

Sherif, M. I., Sultan, M., & Sturchio, N. C. (2019). Chlorine isotopes as tracers of solute origin and age of groundwaters from the eastern desert of Egypt. *Earth and Planetary Science Letters*, *510*, 37–44. https://doi.org/10.1016/j.epsl.2018.12.035

Škerlak, B., Sprenger, M., & Wernli, H. (2014). A global climatology of stratosphere-troposphere exchange using the ERA-Interim data set from 1979 to 2011. *Atmospheric Chemitry and Physics*, *14*(2), 913–937. https://doi.org/10.5194/acp-14-913-2014

Stoertz, G. E., & Ericksen, G. E. (1974). Geology of salars in northern Chile. U.S. Geological Survey Professional Paper, 811.

Sturchio, N. C., Caffee, M., Beloso, A. D. Jr., Heraty, L. J., Böhlke, J. K., Hatzinger, P. B., et al. (2009). Chlorine-36 as a tracer of perchlorate origin. *Environmental Science & Technology*, *43*(18), 6934–6938. https://doi.org/10.1021/es9012195

Suter, M., Beer, J., Bonani, G., Hofmann, H. J., Michel, D., Oeschger, H., et al. (1987). ^{36}Cl studies at the ETH/SIN AMS facility. *Nuclear Instruments and Methods in Physics Research B*, *29*, 211–215. https://doi.org/10.1016/0168-583X(87)90238-2

Synal, H. A., Beer, J., Bonani, G., Suter, M., & Wölfli, W. (1990). Atmospheric transport of bomb-produced ^{36}Cl. *Nuclear Instruments and Methods in Physics Research B*, *52*, 483–488. https://doi.org/10.1016/0168-583X(90)90462-4

Thompson, L. G., Yao, T., Davis, M. E., Henderson, K. A., Mosley-Thompson, E., Lin, P. N., et al. (1997). Tropical climate instability: The last glacial cycle from a Qinghai-Tibetan ice core. *Science*, *276*(5320), 1821–1825. https://doi.org/10.1126/science.276.5320.1821

Tobo, Y., Zhang, D., Nakata, N., Yamada, M., & Iwasaka, Y. (2009). Hygroscopic mineral dust particles as influenced by chlorine chemistry in the marine atmosphere. *Geophysical Research Letters*, *36*, L05817. https://doi.org/10.1029/2008GL036883

Tosaki, Y., Tase, N., Sasa, K., Takahashi, T., & Nagashima, Y. (2012). Measurement of the ^{36}Cl deposition flux in central Japan: Natural background levels and seasonal variability. *Journal of Environmental Radioactivity*, *106*, 73–80. https://doi.org/10.1016/j.jenvrad.2011.11.010

von Engeln, A., & Teixeira, J. (2013). A planetary boundary layer height climatology derived from ECMWF reanalysis data. *Journal of Climate*, *26*, 6575–6590. https://doi.org/10.1175/JCLI-D-12-00385.1

Wahlen, M., Deck, B., Weyer, H., Kubik, P., Sharma, P., & Gove, H. (1991). ^{36}Cl in the stratosphere. *Radiocarbon*, *33*, 257–258.

Wang, B., O'Brien, R. E., Kelly, S. T., Shilling, J. E., & Moffet, R. C. (2015). Reactivity of liquid and semisolid secondary organic carbon with chloride and nitrate in atmospheric aerosols. *The Journal of Physical Chemistry A*, *119*, 4498–4508. https://doi.org/10.1021/jp510336q

Wang, F., Michalski, G., Seo, J. H., & Ge, W. S. (2014). Geochemical, isotopic, and mineralogical constraints on atmospheric deposition in the hyper-arid Atacama Desert, Chile. *Geochimica et Cosmochimica Acta*, *135*, 29–48. https://doi.org/10.1016/j.gca.2014.03.017

Worthington, R. M. (1998). Tropopausal turbulence caused by the breaking of mountain waves. *Journal of Atmospheric and Solar-Terrestrial Physics*, *60*, 1543–1547. https://doi.org/10.1016/S1364-6826(98)00105-9